Reconstitution of the DTX3L-PARP9 complex reveals determinants for high affinity heterodimer formation and enzymatic function

Yashwanth Ashok[1,#,&], Carlos Vela-Rodriguez[1,#], Chunsong Yang[2], Heli I. Alanen[1], Fan Liu[3], Bryce M. Paschal[2] & Lari Lehtiö[1,*]

[1]Faculty of Biochemistry and Molecular Medicine & Biocenter Oulu, University of Oulu, Finland.

[2] Department of Biochemistry and Molecular genetics, University of Virginia, PO Box 800577, Charlottesville, VA22908, USA

[3]Department of Structural Biology, Leibniz-Forschungsinstitut für Molekulare Pharmakologie (FMP), Berlin, Deutschland

[#]These authors contributed equally

[&]Current address: Dept. of Genome Sciences, University of Washington, Seattle, USA

*Corresponding author: Lari Lehtiö – lari.lehtio@oulu.fi

Abstract

In a reaction that requires processing by E1 and E2 enzymes, the E3 ligase complex DTX3L-PARP9 ADP-ribosylates the carboxyl terminus of Ubiquitin and prevents its conjugation to substrate protein. This provides an NAD^+-sensitive mechanism for regulating mono-Ub modification of certain substrates. DTX3L and PARP9 are coordinatedly expressed from a single, bidirectional promoter and can be isolated as a protein complex from multiple cell types. We used purified DTX3L and PARP9, prepared as individual proteins, to investigate how the complex assembles and how complex formation is related to E3 activity. We find that DTX3L binds PARP9 with nanomolar affinity and with an apparent stoichiometry of 1:1. Using a combination of deletion mutants and cross-linking mass spectrometry, we show the interaction involves the D3 domain of DTX3L (230 - 510) and a central region of PARP9 (491 - 630). We found evidence that the DTX3L-PARP9 heterodimer can assemble into a high molecular weight oligomer dependent on the D1 (1 - 100) and D2 (101 - 200) domains of DTX3L. We also show that ADP-ribosylation of Ubiquitin by DTX3L-PARP9 is reversible by several macrodomain-type hydrolases. Our data helps to provide a structural framework for understanding how ubiquitination and ADP-ribosylation are mediated by DTX3L-PARP9.

Introduction

Ubiquitination is a reversible post translational modification of proteins that involves addition of a small protein called ubiquitin (Ub) to target protein lysine residues. Ubiquitination modifies protein properties such as stability, localization, and protein-protein interactions to name a few (reviewed by Swatek & Komander, 2016). Conjugation of a single Ub onto substrate proteins is called monoubiquitination and this process can further proceed by the attachment of additional Ub units resulting in polyubiquitination and formation of Ub chains. Ubiquitination on substrate proteins is achieved by the consecutive action of three enzymes. Ub activating enzyme (E1) uses ATP to activate and transfer Ub to a Ub-conjugating enzyme (E2) that forms a thioester linkage with Ub (E2~Ub). Ubiquitin ligases (E3) recruit E2~Ub complex to transfer Ub onto substrate proteins.

Ubiquitination can be subject to crosstalk with other post-translational modifications such as phosphorylation (Schichl et al., 2011). There is also growing evidence for crosstalk between ubiquitination and ADP-ribosylation (reviewed in Vivelo et al., 2019). ADP-ribosylation is the attachment of ADP-ribose to proteins by enzymes that use NAD^+ as a substrate. ADP-ribose can be transferred as a single unit [mono-ADP-ribose (MAR)] or elongated to polymers of ADP-ribose [poly-ADP-ribose (PAR)]. In humans, majority of intra-cellular ADP-ribosylation is catalyzed by members of the PARP family enzymes.

PARylation has been shown to activate E3 ligases such as RNF146 and Trip21 and modulate cellular processes (Gatti et al., 2020; Kang et al., 2011). Recently, MARylation of Ub on Arg^{42} by bacterial enzymes of SidE family and on Gly^{76} by human DTX3L-PARP9 complex was shown to regulate ubiquitination (Dong et al., 2018; Kamata & Paschal, 2018).

Deltex family of E3 ubiquitin ligases comprises five members; namely DTX1-4 and DTX3L. DTX1, 2 and 4 are characterized by the presence of WWE domains that recognize PAR chains through binding to an iso-ADP-ribose moiety of the chain (Aravind, 2001; Wang et al., 2012). DTX3L, as well as other members of the DTX family, also binds PAR chains through its DTC domain (Ahmed et al., 2020). Furthermore, DTX3L has a unique N-terminal architecture that mediates oligomerization and interaction with PARP9, which in turn binds PAR chains through its macrodomains.

Here we describe the characterization of individually produced DTX3L and PARP9 and demonstrate that the proteins form a high affinity complex. Furthermore, we show that the reconstituted complex has both Ub ADP-ribosylation and ubiquitination activities and subsequently we identified the auto-ubiquitination sites on DTX3L. We also characterized the determinants of the complex formation and were able to show that the complex is mainly formed through interactions between the DTX3L D3 domain and the region of PARP9 preceding the PARP domain. We observed that the C-terminal part of DTX3L is able to ADP-ribosylate ubiquitin in the absence of PARP9, but the activity is enhanced when PARP9 is present.

Results and Discussion

D2 domain is the major determinant of oligomerization

To study the properties of PARP9 and DTX3L, we produced full-length proteins in Sf21 insect cells. We also engineered and expressed several combinations of individual domains (**Fig. 1A**

and Table S1). Purified full-length PARP9 was found to be monomeric based on analytical size exclusion chromatography (aSEC) and SEC-MALS (**Fig. 1B, Fig. S1**). Interestingly, full-length DTX3L appeared to be oligomeric based on the aSEC elution profile (**Fig. 1C**). To identify the domain responsible for DTX3L oligomerization, several deletion constructs were produced. We observed that the N-terminal domains spanning regions D1D2 were oligomeric and in subsequent experiments with smaller D1 and D2 constructs, D2 domain appeared oligomeric (**Fig. 1D**). Cross-linking experiments showed that D2 forms a dimer and potentially some higher molecular weight complexes (**Fig. 1E**). D1 domain alone showed a small amount of dimer formation whereas D1D2 construct revealed higher molecular weight species indicating a pentameric-hexameric assembly with multiple intermediates (**Fig. S2**). Native MS experiments with D1D2 support that the oligomer is not highly stable as we observed formation of a dimer (45 kDa) and tetramer (90 kDa), the latter having less relative abundance. Consistent with crosslinking experiments, native MS with D2 identified only dimeric (23 kDa) and monomeric (11.5 kDa) species, suggesting the contribution of D2 in the formation of a higher oligomer, whereas no oligomers were observed with D1 domains. To further characterize DTX3L oligomer formation, we used small angle X-ray scattering (SAXS) with purified D1D2 domains and full length DTX3L (data not shown for latter). While we observed heterogeneity in the peak for the full-length protein, only some heterogeneity was noted in the peak for D1D2 domains. The relatively low uniformity observed agrees with the cross-linking data, as well as the calculated MWs based on two different methods (114 kDa from PRIMUS and 121 kDa from SAXSMoW) also fit well with the calculated MW of a pentamer (113 kDa) but does not exclude possibility of a hexamer (136 kDa) (**Fig. S3**).

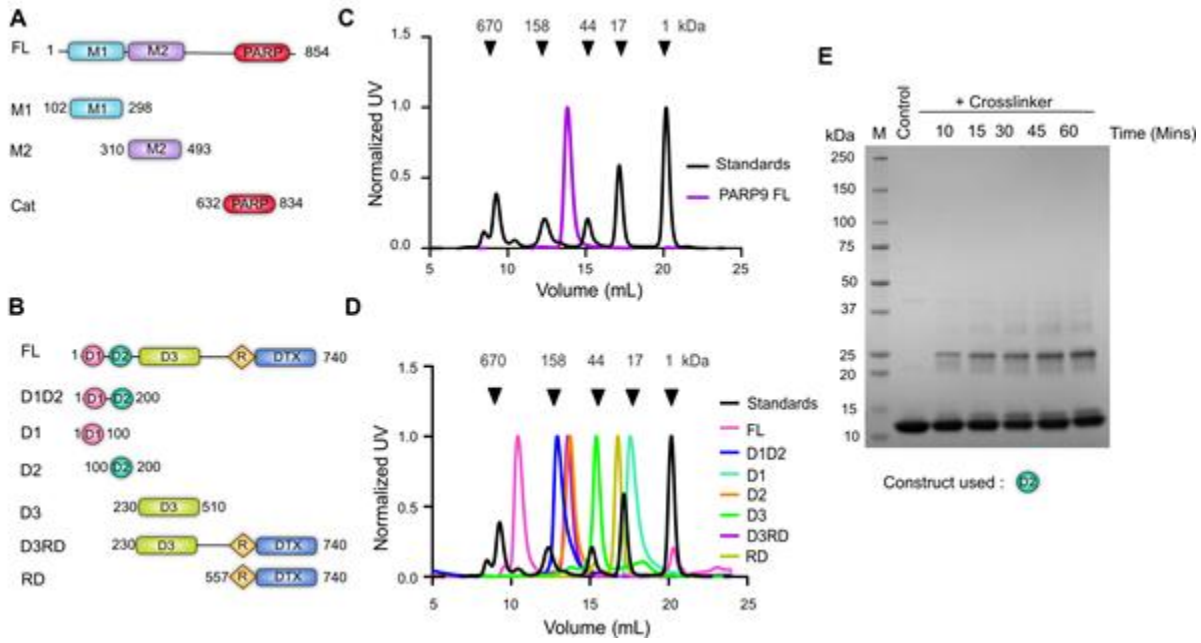

Fig 1. DTX3L and PARP9 domain organization and oligomerization. A, B) Domain organization of PARP9 and DTX3L and constructs used in the studies respectively. C) aSEC analysis of FL PARP9. D) aSEC analysis of various DTX3L constructs. E) Crosslinking analysis of DTX3L D2 domain.

We then used the purified DTX3L constructs to study auto-ubiquitination. All the constructs that contained the RD region (R+DTX) were active in the ubiquitination assay when E1, E2 and ubiquitin were supplied together with ATP (**Fig. 2A**). Time dependent smear formation

due to poly-ubquitination was observed (**Fig. S4**). We then used mass spectrometry (MS) to map ubiquitination sites in DTX3L and were able to identify 34 auto-ubiquitination sites in multiple domains of DTX3L, with the RING domain being the only exception containing no modification sites (**Fig. 2B**). While the extent to which one or multiple ubiquitination sites in DTX3L are utilized in cells is an open question. It is probable that the protein concentration and DTX3L self-association promotes its modification *in vitro*. Ub has 7 lysine residues all of which can be ubiquitinated along with N-terminal methionine creating linear Ub chains. We identified the linkages also by MS and the poly-Ub chains produced by DTX3L are linked though K6, K11, K48 and K63 indicating the potential for DTX3L to modify proteins in the contexts of proteasomal degradation and the DNA damage response (DDR) (Lu et al., 2012; Morris & Solomon, 2004; Paul & Wang, 2017; Wu-Baer et al., 2003) (**Fig. 2B)**. The ubiquitin reaction carried out with Ub with single Lysine mutations and Ub without any lysines (K0) revealed that in all cases DTX3L gets auto-ubiquitinated consistent with multiple possible linkers and/or multiple modifications sites identified within DTX3L (**Fig. 2C**).

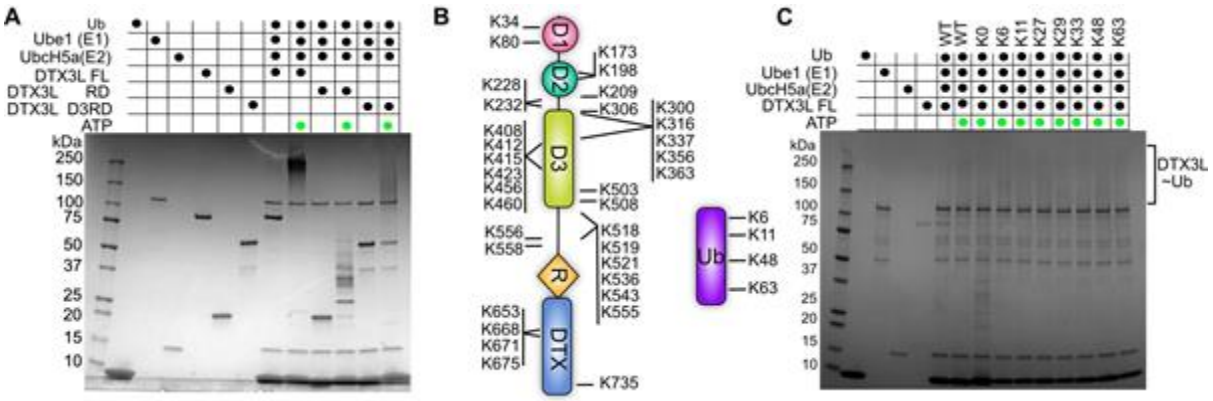

Fig 2: Auto-ubiquitination analysis of DTX3L. A) Constructs containing the RD domain are able to perform ubiquitinating activity. B) Summary of identified ubiquitination sites in DTX3L and ubiquitin linkages using Mass spectrometry. C) Auto ubiquitination of DTX3L with WT Ub and lysine mutant panel.

D3 domain is sufficient for interaction with PARP9

With purified proteins in hand, we then analyzed complex formation between full-length PARP9 and various DTX3L constructs. We used size exclusion chromatography coupled with fluorescently-labelled PARP9, which enabled us to distinguish DTX3L-PARP9 complexes from DTX3L oligomers. As FL DTX3L elutes at an early volume, corresponding to a high molecular weight protein, complex formation with FL PARP9 does not significantly change the elution volume. Therefore, we labelled PARP9 with a fluorophore to aid the visualization of complex formation in size exclusion chromatography. We confirmed that chemical labelling with a fluorophore did not alter elution volume of PARP9 eluting as a monomer (**Fig. S5**). Labelled PARP9 was then mixed with full-length DTX3L and analyzed using size exclusion chromatography (**Fig. 3A**). Fluorophore labelled PARP9 shifts elution volume when incubated with full-length DTX3L indicating complex formation. Therefore, full-length PARP9 readily formed complexes with full-length DTX3L. Subsequent experiments with DTX3L truncations

revealed that D3RD and D3 domain formed complexes with full-length PARP9 (**Fig. 3B,C**). N-terminal D1D2 domains and RD domains of DTX3L were dispensable for complex formation. Similarly, the catalytic domain of PARP9 was unable to form complexes in fluorescence size exclusion chromatography (**Fig. S6**).

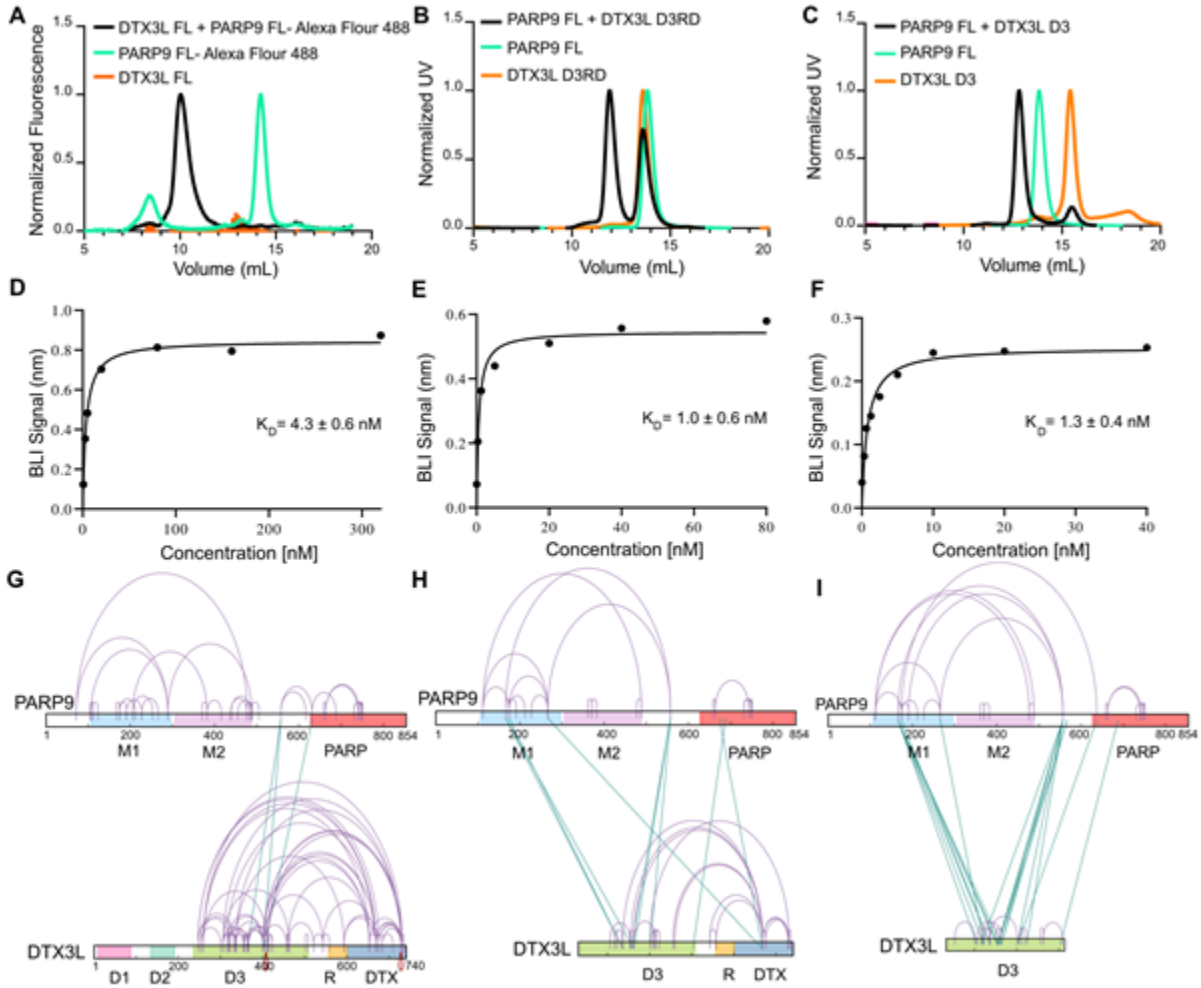

Fig 3. Biochemical studies reveal the protein domains involved in complex formation. Studies with FL PARP9 and FL DTX3L A) aSEC showing complex formation D) Representative BLI binding curve G) XL-MS linkage maps. Experimental results for FL PARP9 and D3RD. B) aSEC showing complex formation E) Representative BLI binding curve H) XL-MS linkage maps. Experimental results with FL PARP9 and D3 domain. C) aSEC showing complex formation F) Representative BLI binding curve I) XL-MS linkage maps. D-F) K_D values are reported as (mean ± SD) (n=3). G-I) Intra-protein links are shown as purple arcs. Inter-protein links are shown as cyan lines between PARP9 and DTX3L. Symmetrical peptide crosslinks (e.g., K408 crosslinked to K408 on another peptide) are shown in red lines.

The complex of the DTX3L-D3 and PARP9 had an apparent 1:1 stoichiometry based on SEC-MALS (**Fig. S1**). We then measured the affinity of complex formation of FL PARP9 with FL DTX3L, D3RD and D3. In all cases the biolayer interferometry showed single digit nanomolar affinities with K_Ds of 1.0 to 4.3 nM (**Fig. 2D-F**). This is in line with the earlier observation that the complex can be extracted from the cells directly (Yang et al., 2017). In order to get further

insight into the complex formation we turned into cross-linking mass spectrometry (XL-MS), a technique where proteins or protein complexes are treated with bifunctional crosslinkers linking physically proximal regions of the protein and analyzing linked peptides after proteolysis.

We performed XL-MS with full-length PARP9 and three different constructs of DTX3L to identify both inter- and intra-molecular contacts at peptide level resolution. Despite evidence of D2 domain mediating oligomerization, we observed no cross-links between D2 domains in full-length context (**Fig. 3G**). This could be interpreted as lack of proximal lysines in the regions that oligomerize. Two cross-linked sites in DTX3L, K408 and K728 were crosslinked to themselves (i.e., a peptide containing K408 was crosslinked to K408 on another peptide), suggesting that these regions at least in context of full-length DTX3L come in proximity with each other, but this is the only direct evidence from cross-linking to an oligomer formation.

For full-length proteins we observed 70 intra-protein cross-links DTX3L and 30 intra-protein crosslinks in PARP9. Three inter-protein peptide cross-links between PARP9 and DTX3L were seen (**Fig. 3G**). These cross-links were observed between the D3 domain of DTX3L and the region located between M2 and PARP domains of PARP9. On the other hand, 49 high confidence intra- and inter-protein cross-links were observed between PARP9 and D3RD domains of DTX3L **(Fig. 3H)**. Of the 49 crosslinks, 18 were PARP9 intra-protein crosslinks, 22 DTX3L intra-protein cross-links and 9 inter-protein crosslinks. With a shorter D3 domain, 21 intra-protein cross-links were seen in PARP9, 12 within D3 domain and 18 inter-protein cross-links **(Fig. 3I)**. Macrodomain M1 does not crosslink in the context of full-length DTX3L but steadily increases cross linked peptides from four for D3RD and seven for D3 domain (**Fig. 3G-I**). These results suggest that longer constructs restrain mobility of the domains with respect to each other. Two inter-protein crosslinks were common for all three DTX3L constructs: PARP9 K557 is a hotspot for interaction with DTX3L D3 domain residues K401 and K363. Overall cross-linking patterns indicate that PARP9 and DTX3L form a compact structure (**Fig. 3G-I**). We used available crystal structures of PARP9 and DTX3L domains to validate crosslinking method (**Fig. S7**).

DTX3L ADP-ribosylates ubiquitin in the absence of PARP9

In our earlier studies (Yang et al., 2017) we reported that the DTX3L-PARP9 complex mediates ADP-ribosylation of Ub on the C-terminal residue Gly^{76}. Using highly pure preparations with individual proteins, we found that ADP-ribosylation of Ub Gly^{76} could be catalyzed by DTX3L alone (**Fig. 4A, lane 3**). Including PARP9 in the reaction, however, enhanced ADP-ribosylation of Ub (**Fig. 4A, lane 4**). The presence of PARP9 also promoted the E3 activity of DTX3L, as indicated by the increased Ub-T7 product formation. An interesting observation was that addition of NAD^+ to the reaction switched on ubiquitination of PARP9 that was otherwise absent. These data suggest that PARP9 contributes to both the ADP-ribosylation and E3 functions of the heterodimer.

A ~200 amino acid C-terminal fragment of DTX3L (aa 557-740) was shown by Chatrin et al. to ADP-ribosylate Ub in vitro (Chatrin et al., 2020). We therefore compared the activities of the DTX3L fragment to that of full-length DTX3L and the DTX3L-PARP9 heterodimer (**Fig. 4B**). The DTX3L fragment is not recognized by the DTX3L antibody used in these assays, but the fragment was detectable via the His-tag. We found that the fragment displays Ub ADP-ribosyl transferase activity that is higher than the full-length heterodimer. This may suggest that the structure of the heterodimer, which includes multiple contacts between DTX3L and

PARP9, helps restrain the biochemical activity of DTX3L. It is plausible that heterodimerization with PARP9 stabilizes DTX3L in a manner that promotes activity, though PARP9 could also have a more direct role in the reaction. We did observe by mass spectrometry crosslinking evidence for contact between the PARP9 catalytic domain and the DTX domain of DTX3L (**Fig. 3H,I**), which suggests a model where both domains contribute to the activity.

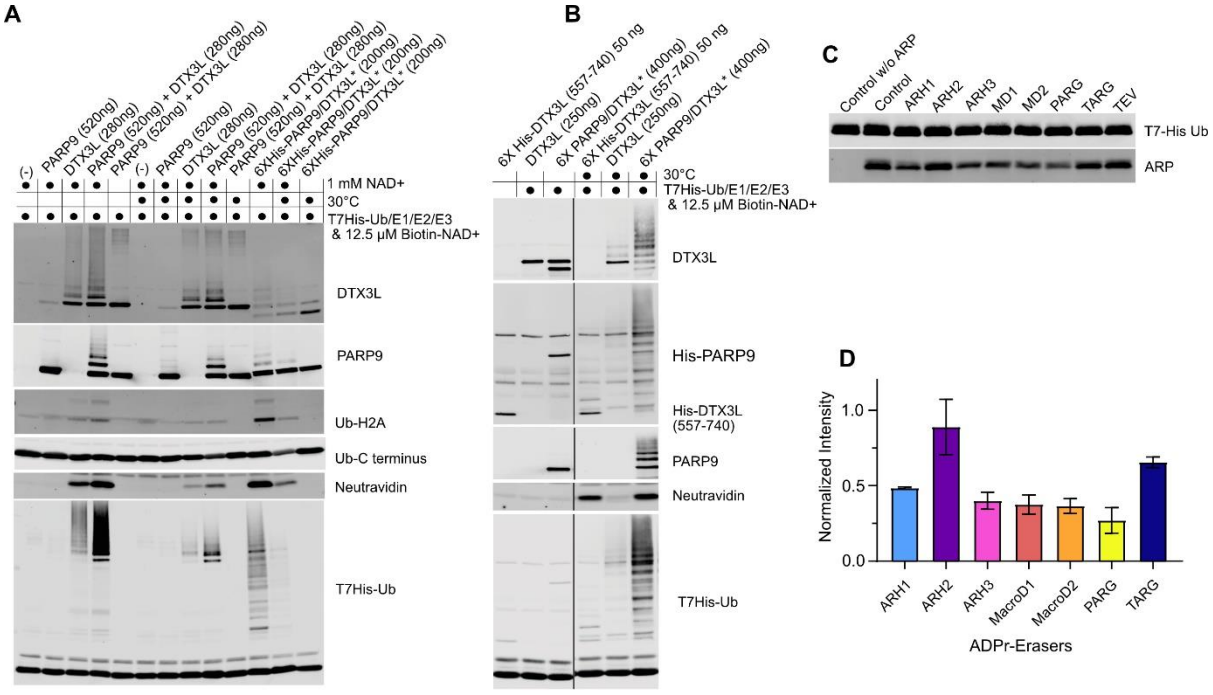

Fig 4. E3 and ADP-ribosyltransferase activities of DTX3L/PARP9. A) Assays with full-length DTX3L and PARP9, individually and after heterodimer reconstitution. Protein components/concentrations are indicated. All reactions contained E1, E2, histone H2A, T7-His6-Ub, ATP, and Biotin-NAD$^+$, and were incubated on ice or at 30°C. A subset of reactions were supplemented with excess NAD$^+$(1 mM). The reaction products were analyzed by immunoblotting with the indicated antibodies. ADP-ribosylation of Ub was detected using fluorescently-labeled Neutravidin, as described (Yang et al., 2017). *Indicates co-expressed heterodimer. B) Assays comparing the DTX3L Ring-DTC domain to full-length DTX3L and DTX3L-PARP9 heterooligomer. The reactions were performed and analyzed essentially as described in Panel A. *Indicates co-expressed heterodimer. C) Hydrolysis of ADP-ribose from the C-terminus of Ubiquitin by a panel of human ADP-ribosylhydrolases. TEV protease was used as a control. D) Quantification of the hydrolysis activity.

Hydrolysis of ADP-ribosyl from Ub

During the completion of this study, it was reported that Ub Gly^{76} ADP-ribosylation can be reversed *in vitro* by deubiquitinases (DUBs) (Chatrin et al., 2020). DUBs are not, however, the typical erasers of ADP-ribosylation and three families of ADP-ribosylation erasers have been reported. The erasers of ADP-ribosylation are grouped in the ARH family of enzymes (comprising ARH1-3), macrodomain containing enzymes (PARG, TARG1, MacroD1 and MacroD2), and nudix hydrolases. Apart from PARG, all erasers are dependent on the amino acid linkage to ADP-ribose. For example, ARH1 targets N-glycosidic bonds on Arginine,

whereas ARH3 targets O-glycosidic bonds on serine (Abplanalp et al., 2017; Fontana et al., 2017; Kato et al., 2007). MacroD1, MacroD2 and TARG1 target ADP-ribose conjugated to acidic residues like glutamic acid and aspartic acid (Chen et al., 2011; Jankevicius et al., 2013; Rosenthal et al., 2013; Sharifi et al., 2013). In contrast to other erasers, nudix are considered as partial hydrolases since they cleave the phosphodiester bond between adenosine and ribose instead of removing complete ADP-ribose units (O'Sullivan et al., 2019).

We analyzed a panel of recombinant ADP-ribosylation erasers for the ability to remove the modification. Our results indicate that most of the enzymes tested can remove ADP-ribose from Ub- Gly^{76} (**Fig. 4C,D**). Both ARH1 and 3 had similar activities, but substrates for ARH2 remain unknown and it did not show any activity towards Ub Gly^{76} ADPr. On the other hand, amongst enzymes that contain a macrodomain fold, MacroD1 and D2 showed high hydrolysis activities. These are *in vitro* studies and the physiological relevance of these erasers and DUBs would require further cell-based experiments.

In summary, we have used biochemical methods to characterize the DTX3L-PARP9 complex. DTX3L binds PARP9 with nanomolar affinity and relies on multiple inter-subunit contacts to help maintain the overall structure and biochemical activity of the complex. We provided evidence for intra-protein contacts within DTX3L, and also within PARP9. The latter included contacts both within and between the two macrodomains of PARP9, which are known to provide the complex with ADP-ribose reader function (Kamata et al., 2021). The coordinated expression and efficient assembly of DTX3L-PARP9 helps to bring together the E3, ADP-ribosyl transferase, and ADP-reader function into a single complex.

Materials and Methods:

Protein expression and purification

Expression vectors pNH-TrxT (#26106), pNIC-CH (#26117), pFastBac1 His-MBP (#30116) were procured from Addgene. pNIC28-MBP was constructed by replacement of TrxT with MBP (Sowa et al., 2020). Throughout the study, Uniprot IDs corresponding to DTX3L (#Q8TDB6-1) and PARP9 (#Q8IXQ6-1) were used. All constructs were verified by dideoxy sequencing. Details of expression constructs are provided in **Table S1**.

Expression constructs were transformed into BL21 (DE3) and selected on appropriate antibiotic selection plates. Overnight culture with 50 µg/ml of kanamycin were grown at 37°C. Terrific Broth-autoinduction media (Formedium, UK) supplemented with 8 g/l glycerol was used for protein expression. Briefly, when the bacterial culture grown at 37°C reached 1 O.D, the incubation temperature was reduced to 18°C for overnight. Cultures were harvested by centrifugation and frozen with lysis buffer until required.

For protein expression in insect cells, recombinant bacmids were transfected into Sf21 cells using Fugene6 (Promega E2693). Supernatant containing viruses (V_0) were harvested after seven days. These viruses were amplified once more to increase the virus titre (V_1). Typically, 1×10^6 cells were used for protein expression using an appropriate volume of V_1 virus that was predetermined to induce growth arrest in small-scale experiments. Cell pellets were harvested 72 hours after growth arrest and frozen at −20°C with lysis buffer before use.

Cell pellets resuspended in lysis buffer (50 mM Hepes pH 7.4, 0.5 M NaCl, 10% glycerol, 0.5

mM TCEP and 10 mM Imidazole) were sonicated and centrifuged at 16,000 rpm to separate soluble material from cellular debris. Filtered supernatant was then loaded to pre-equilibrated HiTrap^{TM} IMAC columns (Cytiva Biosciences). Columns were washed with lysis buffer, followed by wash buffer (50 mM Hepes pH 7.4, 0.5 M NaCl, 10% glycerol, 0.5 mM TCEP and 25 mM Imidazole) and then eluted with elution buffer (50 mM Hepes pH 7.4, 0.35 M NaCl, 10% glycerol, 0.5 mM TCEP and 350 mM Imidazole). For constructs with MBP tag, IMAC elution was loaded into MBP-Trap columns, washed with SEC buffer (30mM Hepes pH 7.5, 0.35 M NaCl, 10% glycerol, 0.5 mM TCEP) and eluted in same buffer with 10 mM maltose. Pooled fractions from MBP column or from other constructs without MBP tag from IMAC were digested with TEV protease (in-house preparation) (van den Berg et al., 2006) with 1:30 (TEV:recombinant protein) molar ratio for 1-2 days followed by reverse IMAC purification to remove TEV and cleaved tags. Proteins collected in the flowthrough were pooled and run in SEC, verified by SDS-PAGE and flash frozen and stored at – 70°C. Protein identity was verified by MALDI-TOF analysis.

Co-expressed DTX3L-PARP9 complex was produced as previously reported (Yang et al., 2017).

aSEC studies

Superdex 200 10/30 increase equilibrated with running buffer (30 mM Hepes pH 7.5, 150 mM NaCl, 5% glycerol, 0.5 mM TCEP) with a flowrate of 0.3 ml was used. BioRad gel filtration calibration kit was used as a standard. Fluorescent labelling was done using DyLight 488 (Thermo) at 9.8 mM. The dye was added to the protein PARP9 FL and PARP9 M1 in an equimolar ratio and incubated for an hour at room temperature kept from the light. Excess dye was removed with a Zeba™ 7 K MWCO spin desalting column (ThermoFisher) equilibrated with running buffer.

Native MS measurements

D1-D2 and D1 were diluted to 10 mg/mL in 20 mM Hepes pH 7.5, 150 mM NaCl, 0.5 mM TCEP and then buffer was exchanged to 200 mM ammonium acetate pH 4.5 with a Zeba™ 7 K MWCO desalting column (ThermoFisher). Proteins were first measured in denaturing conditions by diluting the samples in 50% acetonitrile, 0.1% formic acid. Sample was filtered with Vivaclear mini clarifying filters (0.8µm PES) for 30 sec at 6000rpm. 9 µL from the sample were transferred to a NanoEs spray capillary (Cat no ES380; ThermoScientific). Measurements collected and analysed with BioPharma Finder (ThermoScientific). Native measurements were conducted in the same way as described before with the difference that the protein was diluted in 200 mM ammonium acetate pH 4.5 instead.

Ubiquitination assays

Ubiquitination reactions for DTX3L constructs were prepared in 50 µL volume by mixing (Ube1, E1) 0.4 µM, (Ubc5Ha, E2) 2 µM, DTX3L (0.67 µM) and Ub (45 µM). Tris buffer (1 M, pH 7.5) containing ATP (40 mM), MgCl2 (100 mM) and DTT (40 mM) was added in a 1:20 buffer to reaction volume ratio to initiate ubiquitination. Upon ATP addition, the reaction was incubated at room temperature for up to 2 h. The reaction was quenched by adding 2x

Laemmli buffer at times 0, 15, 30, 60 and 120 min and analyzed using SDS-PAGE and coomassie staining. WT ubiquitin was produced in-house while single lysine ubiquitin and K0 ubiquitin were obtained from LifeSensors (Cat. # SI210).

Identification of Ubiquitination sites

Ubiquitination reactions with DTX3L FL were conducted and resolved with SDS-PAGE. Bands corresponding to modified and unmodified proteins were cut from the gel and washed with 190 mL 40% acetonitrile (ACN) 50 mM ABic buffer until the gel piece is colourless. Then the sample was incubated at room temperature for 60 min with 100 µL of 40% ACN 50 mM ABic buffer and 2 µL 1 M DTT. After adding 4.2 µL of iodoacetamide (IAA), the sample was incubated for 30 more minutes. Following the incubation, gel pieces were washed with 190 µL 40% acetonitrile (ACN) 50 mM ABic buffer and immediately after with 190 µL of sterile water. Liquid was removed from the gel and afterwards 5 µL of trypsin (1/50 T7575, Sigma Aldrich) were added incubating the gel overnight at room temperature.

Trypsin-digested proteins were analyzed by LCMS analysis using an Easy-nLC 1000 system (ThermoFisher Scientific) coupled to a Fusion Lumos Tribrid mass spectrometer (ThermoFisher Scientific). Peptides were trapped on a Symmetry C18 0.18 x 20 mM trap column (Waters) and separated on a Waters M/Z Peptide BEH C18 130 Å 1.7 µm 0.075x150 mm column using a gradient from 97% A (0.1% formic acid) to 35% B (0.1% formic acid in ACN) over 60 min at a flow rate of 0.3 µl/min. The instrument was operated in 3 sec cycles where the MS spectra were recorded with the orbitrap analyzer at resolution of 120000 allowing the collection of up to $4e^5$ ions for maximal 100 msec before switching to MS/MS mode. Multicharged ions (threshold $2.5e^4$) were fragmentated by HCD (30% collision energy) using quadrupole isolation with 1.6 Da width and 15 sec dynamic exclusion. Up to $5e^4$ fragment ions were collected for max 100 msec and analyzed in the orbitrap analyzer at a resolution of 15000. Ions between 1000 and 25000 in intensity were fragmented in the same way but MS/MS scans were recorded in the ion trap (rapid mode) aiming at higher sensitivity (threshold $1e^4$, max 300 msec).

Raw data were and analyzed with Proteome Discoverer 2.2 (ThermoFisher Scientific) using SEQUEST as search engine. MS/MS spectra recorded in the ion trap were processed with a 0.6 Da mass tolerance and data recorded with the orbitrap with a 0.02 Da tolerance. Raw data were recalibrated with the SWISS-PROT human database (9605, v2017-07-05) and after spectrum selection searched against the same database with the following settings: precursor mass tolerance 10 ppm, trypsin cleavage with up to 2 missed cleavages, carbamidomethyl on Cys, oxidation on Met, deamidation on Gln and Asn, protein N-terminus acetylated, and GG adduct on Lys as optional modifications.

Ubiquitin remnant peptides (GG peptides attached to lysine) were identified by searching for +114.042928 Da in lysine residues. Only peptides that showed 100% abundance in ubiquitinated sample when compared to the control sample were taken as ubiquitinated peptides. As trypsin cannot cleave at Ubiquitin modified lysines, peptides with C-terminal K-GG were excluded.

ADP-ribosylation assays

The assays were performed in 20 ml of volume containing 50 mM Tris-HCl (pH 7.5), 50 mM NaCl, 5 mM MgCl2, 1 mM DTT, 0.5 mM ATP, 0.1 mg/ml His6-T7-ubiquitin, 12.5 mM biotin-NAD^+,(-/+ unlabeled β-NAD^+), 10 mg/ml each of Ube1 (E1) and UbcH8 (E2), and 0.25 mg DTX3L alone, 0.05 mg His6-DTX3L(557-740), 0.5 mg PARP9 alone, 0.25 mg DTX3L + 0.5 mg PARP9 mixture (pre-incubated at 4°C for >60 min to form complex), 0.2 mg recombinant DTX3L-(His6)PARP9 purified from bacteria, with or without 2 mg Histone H2A. The reactions were incubated at 30°C for 30 min, quenched by adding 2x Laemmli buffer, separated in SDS-PAGE, and followed with detection by Neutravidin-DyLight-800 (Pierce 22853) for biotin-ADP ribosylated Ub and anti-Ub-H2A (Cell signaling Technology #8240) for H2A ubiquitylation.

Hydrolysis assays

His6-T7-Ub was ADP-ribosylated in the presence of 1 mM unlabeled β-NAD^+. The unreacted β-NAD^+ was removed with Zeba Spin Desalting column (Thermo Scientific #89892). The hydrolyses of ADPr-Ub were performed in 20 mM Tris-HCl (pH 7.5), 50 mM NaCl, 5 mM MgCl2, 2 mM DTT, 0.2 mg/ml BSA and 0.3 mM hydrolase at 37°C for 60 min. ARP (Biotin-containing reagent, Cayman Chemical # 10009350) modification of the remaining ADPr-Ub were carried out in the presence of 1 mM ARP in 0.5 mM acetic acid at room temperature for 60 min (Yang et al., 2017). The reactions were stopped with 2x Laemmli buffer mixed with neutralizing NaOH, separated by SDS-PAGE, and quantified by Neutravidin-DyLight-800 detection.

Crosslinking and XL-MS

Cross linking reactions were carried out at room temperature in 30 mM HEPES buffer, pH 7.5, with 350 mM NaCl, 10% (v/v) glycerol, 0.5 mM TCEP. PARP9 FL was mixed in equimolar ratios with DTX3L D3 and with DTX3L D3RD, at 15 µM and 8.6 µM respectively in 100 µL. To initiate reaction, freshly prepared BS3 (Thermo Scientific, #21580, Lot#OJ192037) was added to a final concentration of 500 µM to each reaction. BS3 was prepared by dissolving 2 mg of BS3 powder in 277 µL of distilled water to make a 12.5 mM working stock solution.

After incubation at appropriate times, aliquots were quenched by addition of 1 M Tris-HCl buffer, pH 8.5 (0.47 mM final concentration) to a 10 µL aliquot taken from the reaction. Samples were incubated for 20 min at room temperature and then analysed by SDS PAGE. Bands of the expected molecular weight for both complexes (PARP9 FL-DTX3L D3 and PARP9 FL-DTX3L D3RD), were recovered from the gel for cross linking mass spectrometry analyses.

Cross linking of D1, D2 and D1D2 was done in a similar manner as the cross-linked complexes. Protein concentration used for these reactions was 0.5 mg/mL and quenching of the reaction was done after 10, 15, 30, 45, and 60 min. Samples were resolved using SDS-PAGE and PageBlue staining (Thermo Scientific).

Cross-linked PARP9-D3 and PARP9-D3RD were loaded on SDS-PAGE and subjected to in-gel digestion. Gel bands were reduced with 5 mM DTT at 56 °C for 30 min and alkylated with 40 mM chloroacetamide at room temperature for 30 min in the dark. Protein digestion was

carried out using trypsin at an enzyme-to-protein ratio of 1:20 (w/w) at 37 °C overnight.

Cross-linked DTX3L-PARP9 were digested in-solution by adding urea (6 M final concentration). The samples were reduced with 5 mM DTT at 37 °C for 60 min and alkylated with 40 mM chloroacetamide at room temperature for 30 min in the dark. Protein digestion was carried out using Lys C at an enzyme-to-protein ratio of 1:75 (w/w) at 37 °C for 4h. After diluting to 2M urea, the digestion was continued with trypsin at an enzyme-to-protein ratio of 1:100 (w/w) at 37 °C and overnight. The samples were cleaned up with C18 stageTip.

LC/MS analysis was performed using an UltiMate 3000 RSLC nano LC system coupled on-line to an Orbitrap Fusion mass spectrometer (Thermo Fisher Scientific). Reversed-phase separation was performed using a 50 cm analytical column (in-house packed with Poroshell 120 EC-C18, 2.7 µm, Agilent Technologies) with a 120 min gradient. Data analysis was performed using pLink 2.3.9 with the following parameters: tryptic in silico digestion with minimum peptide length=6; maximal peptide length=60 and missed cleavages=3; fix modification: Cys carbamidomethyl=57.021 Da; variable modification: Met oxidation=15.995 Da; BS3 crosslinker=138,068 Da. XL-MS figures were generated using xiNET (Combe et al., 2015).

Biolayer interferometry (BLI)

Determination of the affinity parameters was performed using the Octet RED384 (Forté Bio). All binding studies were performed in freshly prepared 30 mM HEPES buffer, pH 7.5, containing 150mM NaCL, 5% (v/v) glycerol, 0.5mM TCEP, 10mg/ml BSA and 0.05% (v/v) Tween 20. The buffer was filtered with a 0.22 µm Minisart® PES syringe filter (Sartorius).

PARP9 FL and heat-inactivated BSA were biotinylated with 1 mM NHS PEG biotin. Biotinylation reaction was incubated for 30 min at room temperature and the excess biotin was removed with a Zeba™ 7k MWCO desalting column (Thermo Scientific).

The affinity measurements were carried out at 30°C using a working volume of 200 µL in black Greiner 96-well flat-bottom plate and 1000 rpm agitation. Eight streptavidin SA Dip and read ™ biosensors (FortéBio) were loaded with biotinylated 20 µg/mL BSA as a reference for nonspecific interactions. Eight streptavidin SA sensors were loaded with 10 µg/mL biotinylated PARP9 FL. Binding affinity was tested with DTX3L D3RD and DTX3L FL at 320, 160, 80, 20, 5, 2.5, 0.625 and 0 nM diluted in the working buffer. The association step was kept for 30 min to ensure signal saturation.

FortéBio Data Analysis HT 11.0 software was used for data analysis. After subtracting the signal from the reference sensors from the signal of the sensors loaded with PARP9 FL, the binding sensorgram was aligned at the beginning of the association step. The sensorgrams were fit using a global model assuming a 1:1 interaction model in steady state.

SAXS data collection and analysis

DTX3L FL (3.9 mg/mL) and D1-D2 (17 mg/mL) were analysed by SEC SAXS at Diamond Light Source B21 beamline (Oxfordshire, United Kingdom). Samples were run by injecting 60 µL to a Superose 6 increase 3.2/300 column at a flowrate of 0.6 mL/min with 30 mM Hepes (pH 7.5), 350 mM NaCl, 5% glycerol, 0.5 mM TCEP. The column was connected to the SAXS

system on the B21 beamline. Based on the Guinier Rg, matching frames from the main peak were averaged. Data processing was done using ScÅtter (Classen et al., 2013) to determine the maximum distance (Dmax), volume and Rg. Molecular weight was determined with Primus (Atsas suite 3.0.3) using the MW and I(0) of BSA (Petoukhov et al., 2012). Additionally, MW was also calculated with the intensity file with the SAXSMoW server (Piiadov et al., 2019). Data for DTX3L FL could not be processed due to the lack of uniformity in the data recorded.

Acknowledgements

We thank Kalle Niemi for testing ubiquitination reactions, Ulrich Bergman for expert help with the native MS and ubiquitin site mapping, Hongmin Tu for expert help with BLI, and beam line scientists at Diamond Light Source B21 beamline for mail-in data collection service. The use of the facilities of the Biocenter Oulu Structural Biology core facility, member of Biocenter Finland, Instruct-ERIC Centre Finland and FINStruct, is gratefully acknowledged. We also thank the Biocenter Oulu Sequencing Center and Proteomics and protein analysis facility. We acknowledge Drs. Opher Gileadi, Cynthia Wolberger and Scott Gradia for making plasmids available through Addgene.

Funding

The research was supported by the Academy of Finland grants 287063, 294085 and 319299 (to LL) and by an NIH grant No. R01CA214872 (to BMP), and by Leibniz Association with the Leibniz-Wettbewerbs (to FL)

Competing interests

The authors declare that they have no competing interests.

References

Abplanalp, J., Leutert, M., Frugier, E., Nowak, K., Feurer, R., Kato, J., Kistemaker, H. V. A., Filippov, D. V., Moss, J., Caflisch, A., & Hottiger, M. O. (2017). Proteomic analyses identify ARH3 as a serine mono-ADP-ribosylhydrolase. *Nature Communications*, *8*(1), 2055. https://doi.org/10.1038/s41467-017-02253-1

Ahmed, S. F., Buetow, L., Gabrielsen, M., Lilla, S., Chatrin, C., Sibbet, G. J., Zanivan, S., & Huang, D. T. (2020). DELTEX2 C-terminal domain recognizes and recruits ADP-ribosylated proteins for ubiquitination. *Science Advances*, *6*(34), eabc0629. https://doi.org/10.1126/sciadv.abc0629

Aravind, L. (2001). The WWE domain: A common interaction module in protein ubiquitination and ADP ribosylation. *Trends in Biochemical Sciences*, *26*(5), 273–275. https://doi.org/10.1016/S0968-0004(01)01787-X

Chatrin, C., Gabrielsen, M., Buetow, L., Nakasone, M. A., Ahmed, S. F., Sumpton, D., Sibbet, G. J., Smith, B. O., & Huang, D. T. (2020). Structural insights into ADP-ribosylation of ubiquitin by Deltex family E3 ubiquitin ligases. *Science Advances*, *6*(38), eabc0418. https://doi.org/10.1126/sciadv.abc0418

Chen, D., Vollmar, M., Rossi, M. N., Phillips, C., Kraehenbuehl, R., Slade, D., Mehrotra, P. V., von Delft, F., Crosthwaite, S. K., Gileadi, O., Denu, J. M., & Ahel, I. (2011). Identification of macrodomain proteins as novel O-acetyl-ADP-ribose deacetylases. *The Journal of Biological Chemistry*, *286*(15), 13261–13271. https://doi.org/10.1074/jbc.M110.206771

Classen, S., Hura, G. L., Holton, J. M., Rambo, R. P., Rodic, I., McGuire, P. J., Dyer, K., Hammel, M., Meigs, G., Frankel, K. A., & Tainer, J. A. (2013). Implementation and performance of SIBYLS: A dual endstation small-angle X-ray scattering and macromolecular crystallography beamline at the Advanced Light Source. *Journal of Applied Crystallography*, *46*(Pt 1), 1–13. https://doi.org/10.1107/S0021889812048698

Combe, C. W., Fischer, L., & Rappsilber, J. (2015). xiNET: Cross-link network maps with residue resolution. *Molecular & Cellular Proteomics: MCP*, *14*(4), 1137–1147. https://doi.org/10.1074/mcp.O114.042259

Dong, Y., Mu, Y., Xie, Y., Zhang, Y., Han, Y., Zhou, Y., Wang, W., Liu, Z., Wu, M., Wang, H., Pan, M., Xu, N., Xu, C.-Q., Yang, M., Fan, S., Deng, H., Tan, T., Liu, X., Liu, L., … Feng, Y. (2018). Structural basis of ubiquitin modification by the Legionella

effector SdeA. *Nature*, *557*(7707), 674–678. https://doi.org/10.1038/s41586-018-0146-7

Fontana, P., Bonfiglio, J. J., Palazzo, L., Bartlett, E., Matic, I., & Ahel, I. (2017). Serine ADP-ribosylation reversal by the hydrolase ARH3. *ELife*, *6*. https://doi.org/10.7554/eLife.28533

Gatti, M., Imhof, R., Huang, Q., Baudis, M., & Altmeyer, M. (2020). The Ubiquitin Ligase TRIP12 Limits PARP1 Trapping and Constrains PARP Inhibitor Efficiency. *Cell Reports*, *32*(5), 107985. https://doi.org/10.1016/j.celrep.2020.107985

Jankevicius, G., Hassler, M., Golia, B., Rybin, V., Zacharias, M., Timinszky, G., & Ladurner, A. G. (2013). A family of macrodomain proteins reverses cellular mono-ADP-ribosylation. *Nature Structural & Molecular Biology*, *20*(4), 508–514. https://doi.org/10.1038/nsmb.2523

Kamata, T., & Paschal, B. (2018). ADP-Ribosylation of the Ubiquitin C-Terminus by Dtx3L/Parp9. *Ubiquitin Proteasome System - Current Insights into Mechanism Cellular Regulation and Disease*. https://doi.org/10.5772/intechopen.81613

Kang, H. C., Lee, Y.-I., Shin, J.-H., Andrabi, S. A., Chi, Z., Gagné, J.-P., Lee, Y., Ko, H. S., Lee, B. D., Poirier, G. G., Dawson, V. L., & Dawson, T. M. (2011). Iduna is a poly(ADP-ribose) (PAR)-dependent E3 ubiquitin ligase that regulates DNA damage. *Proceedings of the National Academy of Sciences*, *108*(34), 14103–14108. https://doi.org/10.1073/pnas.1108799108

Kato, J., Zhu, J., Liu, C., & Moss, J. (2007). Enhanced Sensitivity to Cholera Toxin in ADP-Ribosylarginine Hydrolase-Deficient Mice. *Molecular and Cellular Biology*, *27*(15), 5534–5543. https://doi.org/10.1128/MCB.00302-07

Lu, C.-S., Truong, L. N., Aslanian, A., Shi, L. Z., Li, Y., Hwang, P. Y.-H., Koh, K. H., Hunter, T., Yates, J. R., Berns, M. W., & Wu, X. (2012). The RING finger protein

RNF8 ubiquitinates Nbs1 to promote DNA double-strand break repair by homologous recombination. *The Journal of Biological Chemistry*, *287*(52), 43984–43994. https://doi.org/10.1074/jbc.M112.421545

Morris, J. R., & Solomon, E. (2004). BRCA1: BARD1 induces the formation of conjugated ubiquitin structures, dependent on K6 of ubiquitin, in cells during DNA replication and repair. *Human Molecular Genetics*, *13*(8), 807–817. https://doi.org/10.1093/hmg/ddh095

O'Sullivan, J., Tedim Ferreira, M., Gagné, J.-P., Sharma, A. K., Hendzel, M. J., Masson, J.-Y., & Poirier, G. G. (2019). Emerging roles of eraser enzymes in the dynamic control of protein ADP-ribosylation. *Nature Communications*, *10*. https://doi.org/10.1038/s41467-019-08859-x

Paul, A., & Wang, B. (2017). RNF8- and Ube2S-Dependent Ubiquitin Lysine 11-Linkage Modification in Response to DNA Damage. *Molecular Cell*, *66*(4), 458-472.e5. https://doi.org/10.1016/j.molcel.2017.04.013

Petoukhov, M. V., Franke, D., Shkumatov, A. V., Tria, G., Kikhney, A. G., Gajda, M., Gorba, C., Mertens, H. D. T., Konarev, P. V., & Svergun, D. I. (2012). New developments in the ATSAS program package for small-angle scattering data analysis. *Journal of Applied Crystallography*, *45*(Pt 2), 342–350. https://doi.org/10.1107/S0021889812007662

Piiadov, V., Ares de Araújo, E., Oliveira Neto, M., Craievich, A. F., & Polikarpov, I. (2019). SAXSMoW 2.0: Online calculator of the molecular weight of proteins in dilute solution from experimental SAXS data measured on a relative scale. *Protein Science: A Publication of the Protein Society*, *28*(2), 454–463. https://doi.org/10.1002/pro.3528

Rosenthal, F., Feijs, K. L. H., Frugier, E., Bonalli, M., Forst, A. H., Imhof, R., Winkler, H. C., Fischer, D., Caflisch, A., Hassa, P. O., Lüscher, B., & Hottiger, M. O. (2013).

Macrodomain-containing proteins are new mono-ADP-ribosylhydrolases. *Nature Structural & Molecular Biology*, *20*(4), 502–507. https://doi.org/10.1038/nsmb.2521

Schichl, Y. M., Resch, U., Lemberger, C. E., Stichlberger, D., & de Martin, R. (2011). Novel Phosphorylation-dependent Ubiquitination of Tristetraprolin by Mitogen-activated Protein Kinase/Extracellular Signal-regulated Kinase Kinase Kinase 1 (MEKK1) and Tumor Necrosis Factor Receptor-associated Factor 2 (TRAF2). *The Journal of Biological Chemistry*, *286*(44), 38466–38477. https://doi.org/10.1074/jbc.M111.254888

Sharifi, R., Morra, R., Appel, C. D., Tallis, M., Chioza, B., Jankevicius, G., Simpson, M. A., Matic, I., Ozkan, E., Golia, B., Schellenberg, M. J., Weston, R., Williams, J. G., Rossi, M. N., Galehdari, H., Krahn, J., Wan, A., Trembath, R. C., Crosby, A. H., … Ahel, I. (2013). Deficiency of terminal ADP-ribose protein glycohydrolase TARG1/C6orf130 in neurodegenerative disease. *The EMBO Journal*, *32*(9), 1225–1237. https://doi.org/10.1038/emboj.2013.51

Sowa, S. T., Vela-Rodríguez, C., Galera-Prat, A., Cázares-Olivera, M., Prunskaite-Hyyryläinen, R., Ignatev, A., & Lehtiö, L. (2020). A FRET-based high-throughput screening platform for the discovery of chemical probes targeting the scaffolding functions of human tankyrases. *Scientific Reports*, *10*(1), 12357. https://doi.org/10.1038/s41598-020-69229-y

Swatek, K. N., & Komander, D. (2016). Ubiquitin modifications. *Cell Research*, *26*(4), 399–422. https://doi.org/10.1038/cr.2016.39

Vivelo, C. A., Ayyappan, V., & Leung, A. K. L. (2019). Poly(ADP-Ribose)-Dependent Ubiquitination and its Clinical Implications. *Biochemical Pharmacology*, *167*, 3–12. https://doi.org/10.1016/j.bcp.2019.05.006

Wang, Z., Michaud, G. A., Cheng, Z., Zhang, Y., Hinds, T. R., Fan, E., Cong, F., & Xu, W. (2012). Recognition of the iso-ADP-ribose moiety in poly(ADP-ribose) by WWE domains suggests a general mechanism for poly(ADP-ribosyl)ation-dependent ubiquitination. *Genes & Development*, *26*(3), 235–240. https://doi.org/10.1101/gad.182618.111

Wu-Baer, F., Lagrazon, K., Yuan, W., & Baer, R. (2003). The BRCA1/BARD1 Heterodimer Assembles Polyubiquitin Chains through an Unconventional Linkage Involving Lysine Residue K6 of Ubiquitin*. *Journal of Biological Chemistry*, *278*(37), 34743–34746. https://doi.org/10.1074/jbc.C300249200

Yang, C.-S., Jividen, K., Spencer, A., Dworak, N., Ni, L., Oostdyk, L. T., Chatterjee, M., Kuśmider, B., Reon, B., Parlak, M., Gorbunova, V., Abbas, T., Jeffery, E., Sherman, N. E., & Paschal, B. M. (2017). Ubiquitin Modification by the E3 Ligase/ADP-Ribosyltransferase Dtx3L/Parp9. *Molecular Cell*, *66*(4), 503-516.e5. https://doi.org/10.1016/j.molcel.2017.04.028